KSABC
The Korean Society for Applied Biological Chemistry

Synthesis, characterization, and antioxidant activity in vitro of selenium-*Euryale ferox* Salisb. polysaccharide

Fang Dong[1,2*†] , Hu-Zhe Zheng[1,3†], Woo-Sik Jeong[3], Shin-Kyo Chung[3], Zhong-Yuan Qu[2], Xiang Zou[2,4], Chen Liu[5], Qiong Xiang[1] and Feng Feng[1*]

Abstract

In order to obtain and explore selenide composed of selenium and polysaccharide, three parameters were selected to optimize the synthesis process of selenium-*Euryale ferox* Salisb. polysaccharide (Se-ESPS) by Box-Behnken design. Furthermore, ESPS-B1 separated from ESPS was selenitized to Se-ESPS-B1 by the optimal synthesis process, then the characterization, and antioxidant activity in vitro of Se-ESPS-B1 were explored. The result manifested that the Se content of Se-ESPS was (2.915 ± 0.03) mg/g according to the optimal synthesis process of Se-ESPS (reaction time at 5 h, reaction temperature at 81 ℃, weight ratio of Na_2SeO_3 to ESPS at 0.9 g/g). A series of detection results indicated that the characterizations of Se-ESPS-B1 were apparently distinguished from that of ESPS-B1. Moreover, the antioxidant experiments in vitro demonstrated that Se-ESPS-B1 could exert antioxidant activity by scavenging DPPH, ABTS,·OH, and increasing reduction ability. In conclusion, the synthesis process is an effective approach to harvest selenium-polysaccharide, and Se-ESPS-B1 may be utilized as a potential antioxidant or selenium nutritional supplement.

Keywords: Selenium-*Euryale ferox* Salisb. polysaccharide, Synthesis optimization, Characterization, Antioxidant activity

Introduction

Oxidative stress and peroxidation are regarded as the critical causes of various physical problems [1, 2]. As an essential trace element, selenium has been proved to have a wide range of biological activities, especially in antioxidation [3, 4]. Selenium compounds and selenium enzymes are scavengers of reactive oxygen species (ROS). In chemical experiments, selenium has been found to trap electrophilic ROS [5]. Besides, selenium plays an antioxidant role in human body mainly through selenium enzymes, such as glutathione peroxidase (GPx) and thioredoxin oxidoreductase (TrxR) [6]. GPx with selenocysteine as the active center can catalyze the conversion of reduced glutathione to oxidized glutathione and reduce toxic peroxides to non-toxic hydroxyl compounds [7]. TrxR, which has a unique but essential selenocysteine residue in its C-terminal redox center, can regulate redox reaction, reduce the transcription of pro-inflammatory factors in mitochondria, alleviate oxidative stress, reduce mitochondrial apoptosis and reduce inflammatory response [8–10].

Selenium deficiency in the diet can gradually lead to some diseases, such as Kachin-Beck disease and Keshan disease [11, 12]. Moreover, selenium is a rare and dispersed element, which is mainly in the inorganic form. However, the therapeutic dosage of inorganic selenium is close to the toxic dosage, and the direct absorbability of inorganic selenium has the great safety risks [13].

Euryale ferox Salisb. is cultivated in the pool and marsh of southern China, and its kernel is utilized as common

*Correspondence: dong1234fang@126.com; 20171018@jsfpc.edu.cn
†Fang Dong and Hu-Zhe Zheng contributed equally to this work
[1] School of Health Sciences, Jiangsu Food and Pharmaceutical Science College, Huai'an 223003, China
Full list of author information is available at the end of the article

Dong *et al. Appl Biol Chem*　　(2021) 64:59

Page 2 of 14

food and traditional Chinese medicine for benefitting the body and treating chronic diseases such as diabetes and nephritis by reducing the body's peroxidation level [14]. The evidences show that the important reason for the biological activity of the kernel of *Euryale ferox* Salisb. is that it contains considerable active polymers, namely polysaccharides [15, 16].

The combination of inorganic selenium with polysaccharide is considered to be more bioactive and safer for humans [17]. Besides, it is believed that the biological safety and activity of the physical mixture of inorganic selenium and polysaccharide is lower than that of selenium-polysaccharide due to the conversion of inorganic selenium to organic selenium [18]. Unfortunately, the natural selenium-polysaccharide is scarce in nature. To efficiently harvest selenium-polysaccharide, continuous attention has been paid to the chemical synthesis of selenium-polysaccharide [19–21]. Compared with that of polysaccharide, the microstructure of selenium-polysaccharide may be changed. Furthermore, it is a consensus that the activity of polysaccharide and its microstructure are strongly linked [22–24].

Therefore, we engaged Box-Behnken design (BBD) to optimize the synthesis of selenium-*Euryale ferox* Salisb. polysaccharide (Se-ESPS) and explored the variations on the characterization and antioxidant activity in vitro.

Materials and methods
Sample material
The kernels of *Euryale ferox* Salisb., were collected from Hung-tse Lake in Huai'an, Jiangsu Province, China, and stored at room temperature after drying in air.

Extraction, purification, and isolation of ESPS
The dried kernels of *Euryale ferox* Salisb. were reflux treated by n-hexane for 1 h, 3 cycles to remove nonpolar impurities. Then, the treated kernels were extracted by the water reflux method. The protein of the water extract was removed by Sevag solution and the pigment was removed by macroporous resin D301R. After that, the absolute alcohol was added into the water extract with protein and pigment removed until the final volume of ethanol was 90%. Twenty four hours later, the polysaccharide was centrifuged and collected, named ESPS. Further, ESPS was isolated by DEAE-52 cellulose column and SephadexG-150 with 0.05 mol/L NaCl solution. The eluent was dialyzed to Cl^- free by distilled water, and then freeze-dried to harvest the high-purity polysaccharide, named ESPS-B1. In this paper, ESPS was used in the selenization optimization process and Se-ESPS-B1 was used in analysis of the characterization and antioxidant activity in vitro.

Selenization process
ESPS and Na_2SeO_3 in a certain proportion were put in the Erlenmeyer flask with 200 mL 0.05% HNO_3 solution. Immediately, the mixed solution sealed in the Erlenmeyer flask was reacted at the stated time and temperature in water bath oscillator. After adjusting its pH value of 5–6 with Na_2CO_3, the solution that had completed the selenization reaction was dialyzed by dialysis bag (M_w cut-off: $8 \times 10^3 - 14 \times 10^3$) with tap water for 72 h and purified water for 24 h [18]. When dialysis solution did not present red color after the addition of ascorbic acid, indicating that there was no free SeO_3^{2-}, the Se-ESPS solution was freeze-dried.

Single-factor design of Se-ESPS
Reaction time (3, 4, 5, 6, 7 h), reaction temperature (50, 60, 70, 80, 90 ℃), and weight ratio of Na_2SeO_3 to ESPS (0.2, 0.4, 0.6, 0.8, 1.0 g/g) were investigated as the independent variables in the single-factor experiments. The Se content as dependent variable was gotten on the basis of the linear regression equation ($Y = 105.8X + 2.9$, $R^2 = 0.9999$) of selenium standard solution (National standard sample No. GSB 04-1751-2004, Beijing General Research Institute of Nonferrous Metals, China), which was measured at 196.026 nm by Varian710-ES ICP-OES (Varian Inc., USA).

Box-Behnken design of Se-ESPS
In the light of the results of single factor investigation, three levels were selected from the three factors, shown in Table 1. Box-Behnken design was used to carry out response surface optimization by Design-Expert 7.0 software (Stat-Ease, USA) [25–27].

Appearance observation
Se-ESPS-B1 and ESPS-B1 were placed on the white paper. The color, morphology and other appearance were observed under sunlight.

Infrared spectroscopy
1–2 mg Se-ESPS-B1 and ESPS-B1 were merged with 100–200 mg KBr respectively. The infrared spectra of samples were measured at the 4000–500 cm^{-1} byNicolet380 FTIR (Thermo Fisher Scientific, USA).

Table 1 Codes schedule of variables using BBD

Variables	Code and level		
	− 1	0	+ 1
X_1, reaction time (h)	4	5	6
X_2, reaction temperature (℃)	70	80	90
X_3, mass ratio of Na_2SeO_3 to ESPS (g/g)	0.6	0.8	1.0

Dong *et al. Appl Biol Chem*   (2021) 64:59

Page 3 of 14

Thermogravimetric detection

Se-ESPS-B1 and ESPS-B1 were detected by TGA2 thermogravimetric analyzer (METTLER TOLEDO International Co., Ltd., Switzerland). Detection Parameters: air flow rate 50 mL/min, heating rate 10 ℃/min, temperature range 30–800 ℃.

X-ray diffraction detection

Se-ESPS-B1 and ESPS-B1 were determined by D8AdvanceX-ray diffractometer (Bruker Corporation, Germany). (Detection Parameters: $2\theta = 5°–80°$, room temperature).

X-ray photoelectron spectroscopy detection

The dried and fully ground Se-ESPS-B1 and ESPS-B1 were detected by the K-alpha X-ray photoelectron spectrometer (Thermo Fisher Scientific, USA). Detection parameters: sample thickness less than 5 mm, cone-shaped double anode Mg Kα rays, 12 kV, 180 W, background vacuum 1×10^{-6} Pa in the analysis room, contaminated C1s (Be = 284.6 eV) used for charge correction.

Scanning electron microscope observation

After being sprayed with Au, Se-ESPS-B1 and ESPS-B1 were observed by FEG450 scanning electron microscope (FEI Company, USA).

DPPH radical scavenging capacity

1 mL Se-ESPS-B1 with different concentrations (0.2, 0.4, 0.6, 0.8, 1.0 mg/mL) were merged with 1 mL 0.5 mmol/mL DPPH solution and 10 mL 60% ethanol respectively. After standing at normal atmospheric temperature and away from light for 0.5 h, the absorbance was determined at 517 nm by UV-5200 UV–Vis spectrophotometer (Shanghai Metash Instrument Co., Ltd., China) [28]. The operating procedures of ascorbic acid and ESPS-B1 were the same as that of Se-ESPS-B1. The calculation formula was shown as follows:

$$X = \left[\frac{A_0 - (A_i - A_j)}{A_0} \right] \times 100\% \qquad (1)$$

In formula 1, X is DPPH radical scavenging rate; A_0 is the absorbance value of sample blank control group. A_i is the absorbance value of the sample group; A_j is the absorbance value of the DPPH blank control group.

ABTS radical scavenging capacity

1 mL Se-ESPS-B1 with different concentrations (0.2, 0.4, 0.6, 0.8, 1.0 mg/mL) were merged with 6 mL ABTS working solution which was obtained from ABTS stock solution prepared by equal volume of 7.4 mmol/mL ABTS solution and 2.6 mmol/mL $K_2S_2O_8$ solution. After avoiding light at normal temperature for 6 min, the absorbance was determined at 734 nm by UV-5200 UV–Vis spectrophotometer [29]. The operating procedures of ascorbic acid and ESPS-B1 were the same as that of Se-ESPS-B1. The calculation formula was the same as formula 1. X is ABTS radical scavenging rate; A_0 is the absorbance value of the sample blank control group. A_i is the absorbance value of the sample group; A_j is the absorbance value of the ABTS blank control group.

·OH radical scavenging capacity

1 mL Se-ESPS-B1 with different concentrations (0.2, 0.4, 0.6, 0.8, 1.0 mg/mL) were merged with 2 mL 5 mmol/mL $FeSO_4$ solution, 2 mL distilled water 2 mL 5 mmol/mL salicylic acid ethanol solution and 2 mL 5 mmol/mL H_2O_2 solution. 30 min later, the absorbance was detected at 510 nm by UV-5200 UV–Vis spectrophotometer [30]. The operating procedures of ascorbic acid and ESPS-B1 were the same as that of Se-ESPS-B1. The calculation formula was the same as formula 1. X is ·OH radical scavenging rate; A_0 is the absorbance value of the sample blank control group. A_i is the absorbance value of the sample group; A_j is the absorbance value of the H_2O_2 blank control group.

Total reduction capacity

1 mL Se-ESPS-B1 with different concentrations (0.2, 0.4, 0.6, 0.8, 1.0 mg/mL) were merged with 1 mL 1% (w/v) $K_3[Fe(CN)_6]$ and 1 mL PBS (pH = 6.6). After 20 min reaction at 50 ℃, the reaction solution was added with 2 mL 0.3% trichloroacetic acid. Then, 2 mL mixed solution added with 2 mL distilled water and 0.4 mL0.3% (w/v) $FeCl_3$ was reacted at 50 ℃ for 10 min [31]. The absorbance was detected at 700 nm by UV-5200 UV–Vis spectrophotometer. The operating procedures of ascorbic acid and ESPS-B1 were the same as that of Se-ESPS-B1. The calculation formula was shown as follows:

$$X = A_1 - A_2 \qquad (2)$$

In formula 2, X is the reduction capacity; A_1 is the absorbance value of the sample group; A_2 is the absorbance value of the blank group.

Statistical analysis

The experiments were executed in triplicate, and the results were presented as $\bar{x} \pm s$. Values were evaluated by analysis of variance (ANOVA).

Dong *et al. Appl Biol Chem*   (2021) 64:59

Page 4 of 14

Fig. 1 Effects of different factors on Se-ESPS synthesis. **a** Fixed conditions: reaction temperature 50 ℃, weight ratio of Na_2SeO_3 to ESPS 0.2 g/g; **b** fixed conditions: reaction time 5 h, weight ratio of Na_2SeO_3 to ESPS 0.2 g/g; **c** fixed conditions: reaction time 5 h, reaction temperature 80 ℃
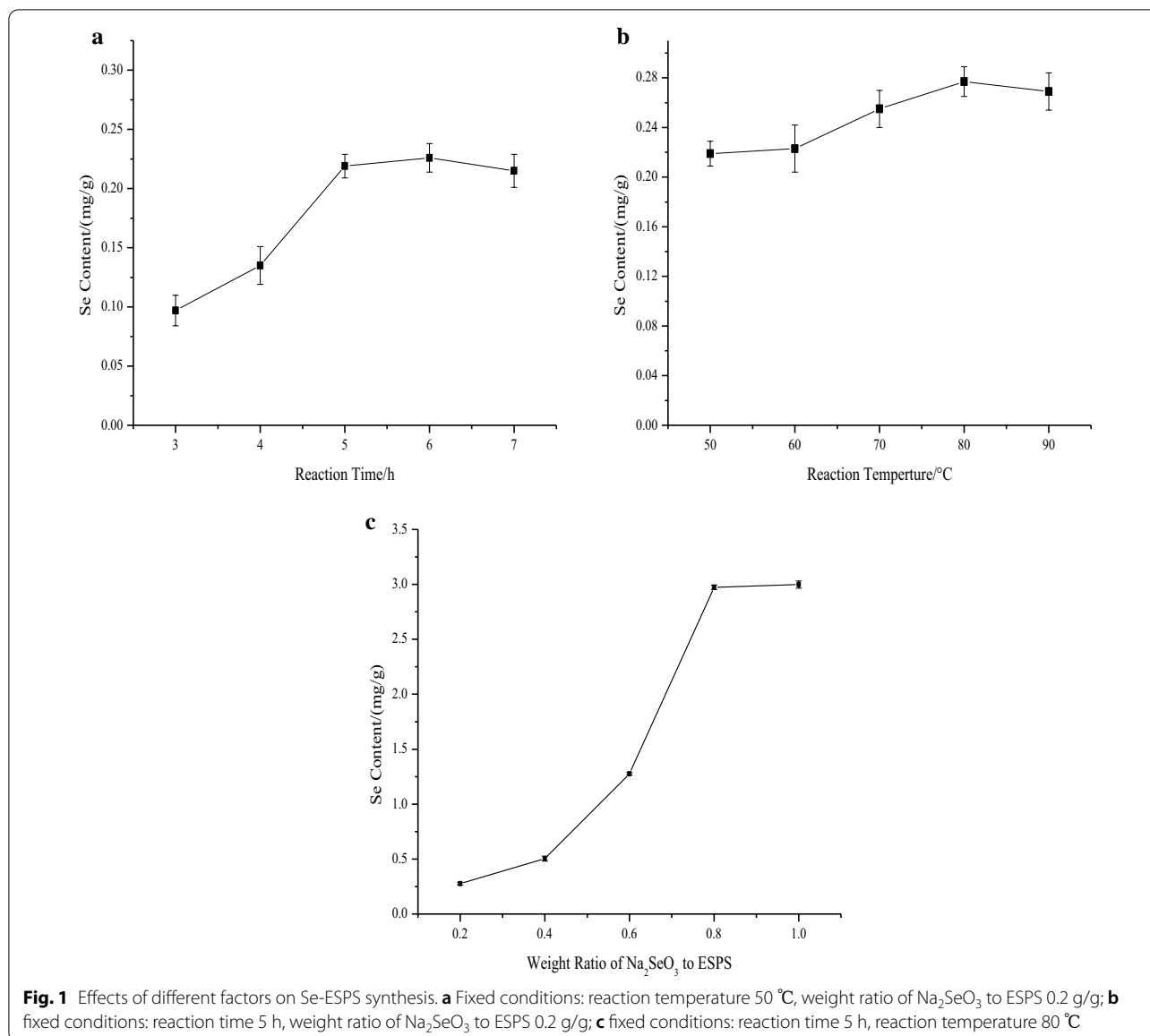
Results and discussion

Single-factor assays

Figure 1a illustrated that Se content of Se-ESPS gradually raised within 3–6 h, but decreased at 7 h. Similarly, the Se content of Se-ESPS rapidly increased in the range of 60–80 ℃ while slightly decreased at 90 ℃, shown in Fig. 1b. The main reason for the above results was that the excessive reaction time and temperature led to the monosaccharide and oligosaccharide combined with Se were hydrolyzed from ESPS, and were dialyzed out from the solution [32]. Therefore, given saving time and energy, 4 − 6 h and 60 − 80 ℃ were selected as levels in

BBD optimization. Figure 1(c) displayed that when the weight ratio of Na_2SeO_3 and ESPS reached 1.0 g/g, the Se content of Se-ESPS slowly increased. The reason was that when the weight ratio of Na_2SeO_3 to ESPS reached a certain proportion, the combining rate of Na_2SeO_3 and ESPS was saturated, and the increasing Na_2SeO_3 could not significantly improve the combining rate [32]. Herein, 0.6 − 1.0 g/g was adopted for the BBD optimization.

Optimized selenization results of Se-ESPS by BBD

The selenization response surface scheme and results are shown in Table 2. Box-Behnken design provided 17

Dong *et al. Appl Biol Chem*   (2021) 64:59

Page 5 of 14

Table 2 Selenization schemes by Box-Behnken design and the responsive results

No.	Factors and levels			Se Content of Se-ESPS (mg/g)
	X_1 (h)	X_2 (℃)	X_3 (g/g)	
1	4	70	0.8	0.793
2	6	70	0.8	1.205
3	4	90	0.8	0.959
4	6	90	0.8	1.592
5	4	80	0.6	0.611
6	6	80	0.6	1.418
7	4	80	1.0	1.755
8	6	80	1.0	1.693
9	5	70	0.6	0.759
10	5	90	0.6	1.286
11	5	70	1.0	1.907
12	5	90	1.0	2.301
13	5	80	0.8	2.974
14	5	80	0.8	2.797
15	5	80	0.8	2.916
16	5	80	0.8	2.865
17	5	80	0.8	2.951

experiments, including factorial experiments No. 1–12 and central experiments No. 13–17. The Se content of Se-ESPS ranged from 0.611 to 2.974 mg/g. Then, the quadratic multinomial regression equation that reflected the relationship between reaction factors and Se content of Se-ESPS was obtained by multiple regression analysis, shown in formula 3.

$$\begin{aligned} Y = {}& 2.90 + 0.22X_1 + 0.18X_2 \\ & + 0.45X_3 + 0.055X_1X_2 \\ & - 0.22X_1X_3 - 0.033X_2X_3 \\ & - 0.98X_1^2 - 0.78X_2^2 - 0.55X_3^2 \end{aligned} \quad (3)$$

Model fitting and analysis

The results of the regression model analysis were shown in Table 3. F value (74.51) and P value (< 0.0001) meant that the model owned the high statistical significance. Moreover, R^2 (0.9879), $AdjR^2$ (0.9764), and Adeq precision (> 4) indicated the high fitting degree of the model. The low value of C.V.% (7.16) showed the high accuracy and reliability of the model [33]. F value (6.44) and P value (0.0817) of lack of fit suggested the few variations between the actual and predicted values [34]. All the above illustrated that the model was accurate and reliable. According to the P values of each model terms, the linear coefficients (X_1, X_2, X_3), secondary coefficients (X_1^2, X_2^2, X_3^2), and interactive coefficient (X_1X_3) significantly influenced selenization (P < 0.01, P < 0.05), while the interaction coefficients (X_1X_2, X_2X_3) had no significant effect on selenization (P > 0.05).

Interactions of parameters in Se-ESPS

Figure 2 showed the 3D surface response plots about the interactions of different parameters. In general, if the 2D contour plot formed by 3D mapping to the bottom plane is more elliptical, the interaction between the two parameters will be more significant [35]. As Fig. 2a shown, the Se content of Se-ESPS initially increased

Table 3 Variance analysis of optimization of selenization of ESPS

Source	Sum of squares	Df	Mean square	Standard error	F value	P value
Model	11.26	9	1.25	–	74.51	< 0.0001[**]
X_1	0.40	1	0.40	0.046	23.85	0.0018[**]
X_2	0.27	1	0.27	0.046	16.17	0.0050[**]
X_3	1.60	1	1.60	0.046	95.52	< 0.0001[**]
X_1X_2	0.012	1	0.012	0.065	0.73	0.4220
X_1X_3	0.19	1	0.19	0.065	11.24	0.0122[*]
X_2X_3	4.422E-003	1	4.422E-003	0.065	0.26	0.6236
X_1^2	4.03	1	4.03	0.063	240.18	< 0.0001[**]
X_2^2	2.59	1	2.59	0.063	154.40	< 0.0001[**]
X_3^2	1.29	1	1.29	0.063	76.60	< 0.0001[*]
Residual	0.12	7	0.017	–	–	–
Lack of fit	0.097	3	0.032	–	6.44	0.0817
Pure error	0.020	4	5.014E-003	–	–	–
Cor total	11.38	16	–	–	–	–

C.V.% = 7.16, R^2 = 0.9897, $AdjR^2$ = 0.9764, Adeq Precision = 24.351

[*] P < 0.05; [**] P < 0.01

Dong *et al. Appl Biol Chem*   (2021) 64:59

Page 6 of 14

Fig. 2 3D response surface plots about the interactions of different parameters
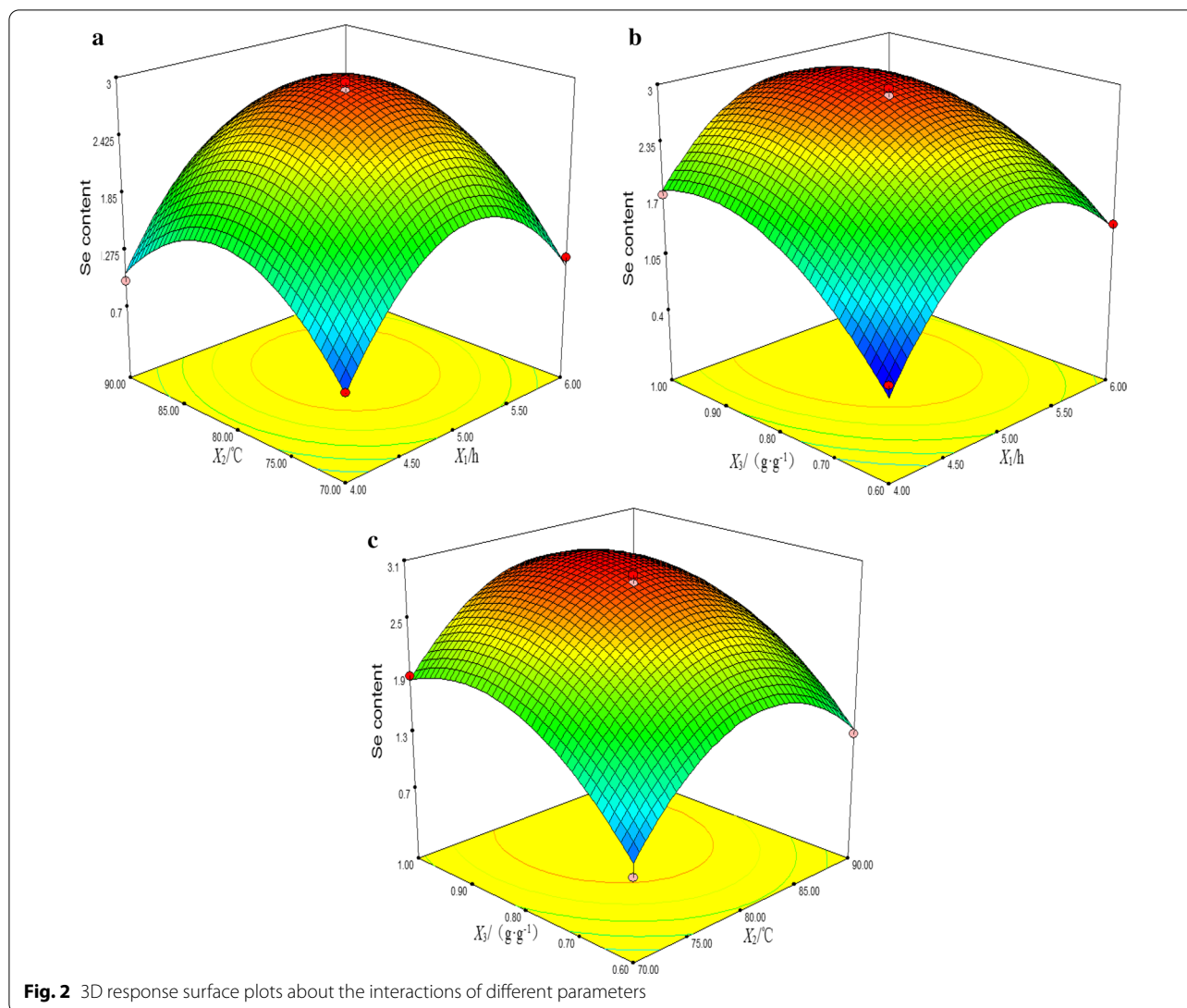
with reaction time (X_1) prolongation and reaction temperature (X_2) increasing, but then decreased. Figure 2b revealed that the Se content of Se-ESPS raised with the increase of weight ratio of Na_2SeO_3 to ESPS (X_3), while the content of Se-ESPS presented a trend of rising first and then falling with reaction time (X_1) prolongation. A similar behavior was also presented in Fig. 2c about the interaction.

Furthermore, the 2D contour plot of Fig. 2b was elliptical, which meant that the interaction between reaction time (X_1) and weight ratio of Na_2SeO_3 to ESPS (X_3) was significant (X_1X_3, P < 0.05, shown in Table 3).

Optimal process and verification experiment
According to the model, the optimal process of Se-ESPS was obtained: the reaction time, the reaction temperature, the weight ratio of Na_2SeO_3 to ESPS was 5.07 h,

81.11 ℃, 0.88 g/g, respectively, and the predicted Se content in Se-ESPS was 3.006 mg/g. For verifying the accuracy and reliability of the optimal selenization process, the proposed process was corrected as follows: the reaction time was 5 h, the reaction temperature was 81 ℃, and the weight ratio of Na_2SeO_3 to ESPS was 0.9 g/g. Based on the corrected process, the Se content of Se-ESPS was (2.915 ± 0.03) mg/g. The actual result approached the prediction, which indicated that the Se-ESPS optimization process was feasible, and the model was accurate and reliable, which could be used for the subsequent selenization experiments. Se-ESPS-B1 was obtained by the optimal process model and the Se content of Se-ESPS-B1 was 3.029 mg/g.

Fig.3 Appearance of Se-ESPS-B1 (**a**) and ESPS-B1 (**b**)
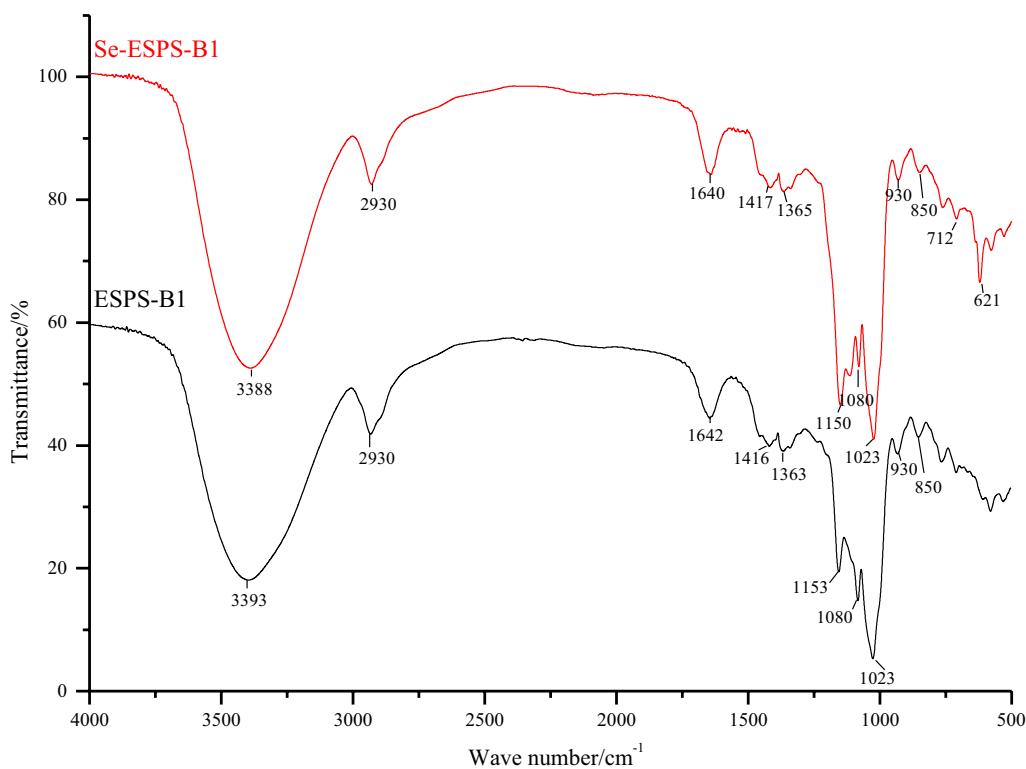
Fig. 4 FTIR spectra of Se-ESPS-B1 and ESPS-B1

Appearance results

As shown in Fig. 3, Se-ESPS-B1 was pink fluffy floc and ESPS-B1 was a white flake. It implied that the structure of Se-ESPS-B1 had changed to some extent after selenization, compared with ESPS-B1.

Dong *et al. Appl Biol Chem*   (2021) 64:59

Page 8 of 14

FTIR analysis

As shown in Fig. 4, both Se-ESPS-B1 and ESPS-B1 had three typical absorption peaks of polysaccharides near 3390, 2930, 1641 cm^{-1}, which were attributed to O–H, C–H stretching vibration, and C=O asymmetric stretching [36], respectively. Two absorption peaks near 1417, 1365 cm^{-1} were attributed to the C-H in-plane bending vibration of Se-ESPS-B1 and ESPS-B1. The absorption peaks near 1150, 1080, 1023 cm^{-1} were C–O–C and C–O–H stretching vibrations of polysaccharides with pyran rings, which indicated Se-ESPS-B1 and ESPS-B1 were pyran ring polysaccharides. In addition, the absorption peaks near 850 cm^{-1} and 930 cm^{-1} were α-glycosidic and β-glycosidic bonds

of Se-ESPS-B1 and ESPS-B1 [37]. However, Se-ESPS-B1 had distinctive absorption peaks at 712 cm^{-1} and 620 cm^{-1}, which were attributed to Se=O and C–O–Se stretching vibrations [37]. The above result showed that selenium was introduced into ESPS-B1 in the forms with Se=O and C–O–Se.

Thermogravimetric assays

It could be seen from Fig. 5 that the TG and DTG curves of Se-ESPS-B1 and ESPS-B1 were similar. Obvious weight loss occurred in the range of 50–100 ℃ for Se-ESPS-B1 and ESPS-B1, which was mainly caused by the evaporation of water contained in Se-ESPS-B1 and ESPS-B1, and the weight loss was about 10% [38].
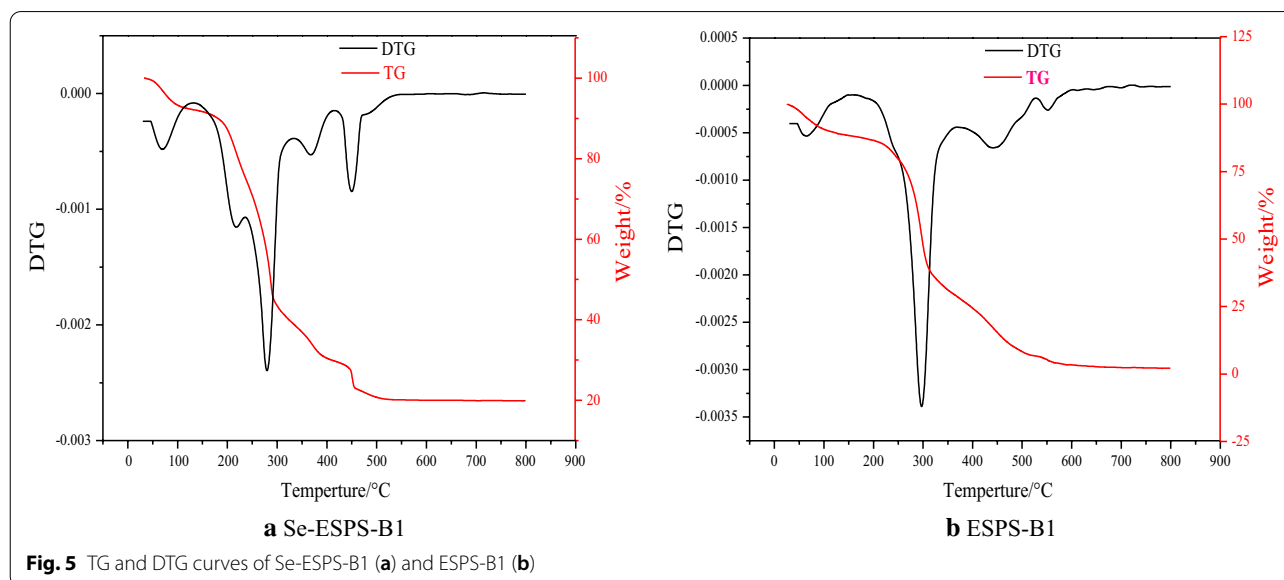
Fig. 5 TG and DTG curves of Se-ESPS-B1 (**a**) and ESPS-B1 (**b**)
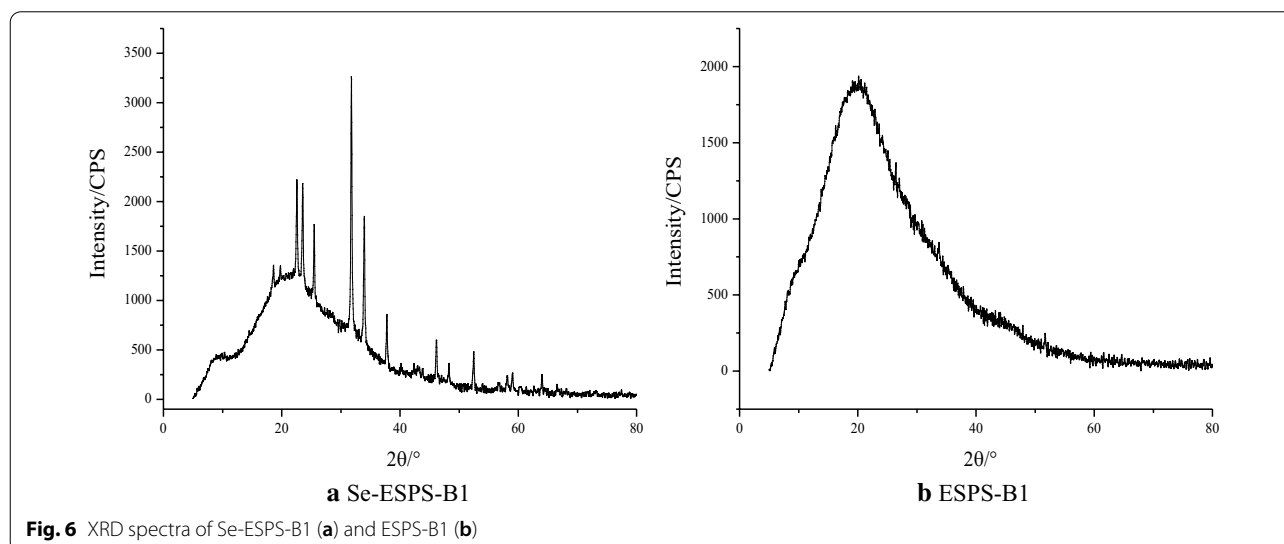
Fig. 6 XRD spectra of Se-ESPS-B1 (**a**) and ESPS-B1 (**b**)

Dong *et al. Appl Biol Chem*   (2021) 64:59

Page 9 of 14

Figure 5a showed that the weight loss rate of Se-ESPS-B1 increased rapidly with the gradual increase of temperature. The maximum weight loss was in the range of 200–350 ℃, and the weight loss was about 65%. In particular, the weight loss was most severe at 278 ℃, indicating that Se-ESPS-B1 was violently decomposed within this range. Similarly, ESPS-B1 decomposed violently in the range of 250–370 ℃, especially at 297 ℃, and the weight loss rate of ESPS-B1 was about 60%, shown in Fig. 5b. From the above analysis, it could be concluded that the thermal stability of Se-ESPS-B1was lower than that of ESPS-B1.

X-ray diffraction assays

As shown in Fig. 6, Se-ESPS-B1 owned obvious diffraction peaks in the range of 20°−40°, indicating that it has the crystal structure, while ESPS- B1 has no diffraction peak in that range, indicating that ESPS-B1 was amorphous [39]. It was suggested that the structure of Se-ESPS-B1 significantly changed after selenization, compared with that of Se-ESPS-B1.

X-ray photoelectron spectroscopy assays

From the X-ray photoelectron spectra of Se-ESPS-B1 and ESPS-B1 in Fig. 7, it could be seen that both of them have

Fig. 7 XPS spectra of Se-ESPS-B1 (**a**) and ESPS-B1 (**b**)

Fig. 8 Se3d core level spectra of Se-ESPS-B1 (**a**) and ESPS-B1 (**b**)

Dong *et al. Appl Biol Chem*   (2021) 64:59

Page 10 of 14
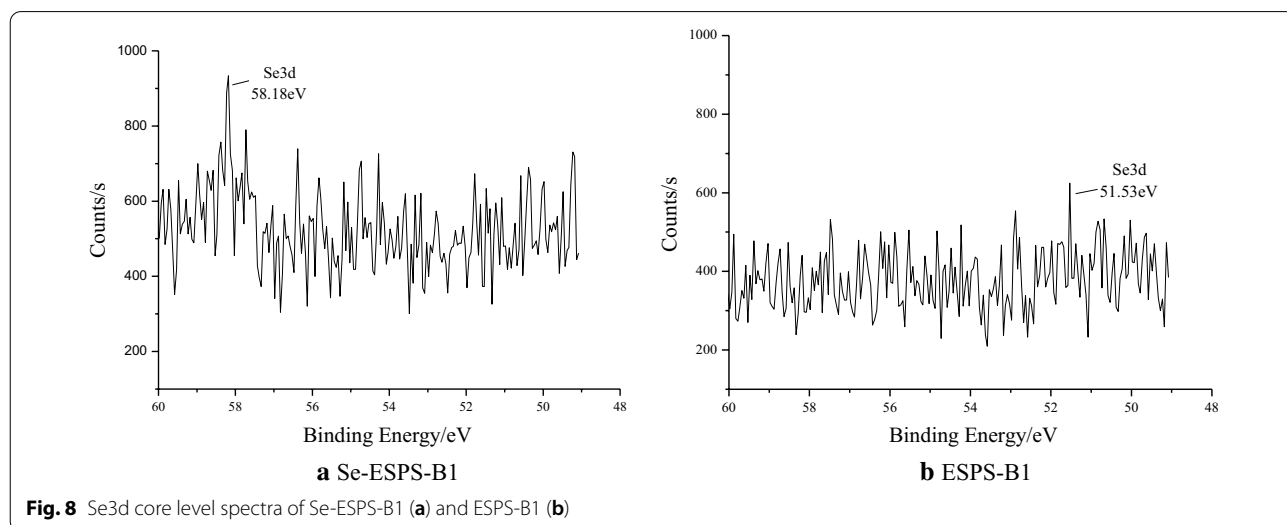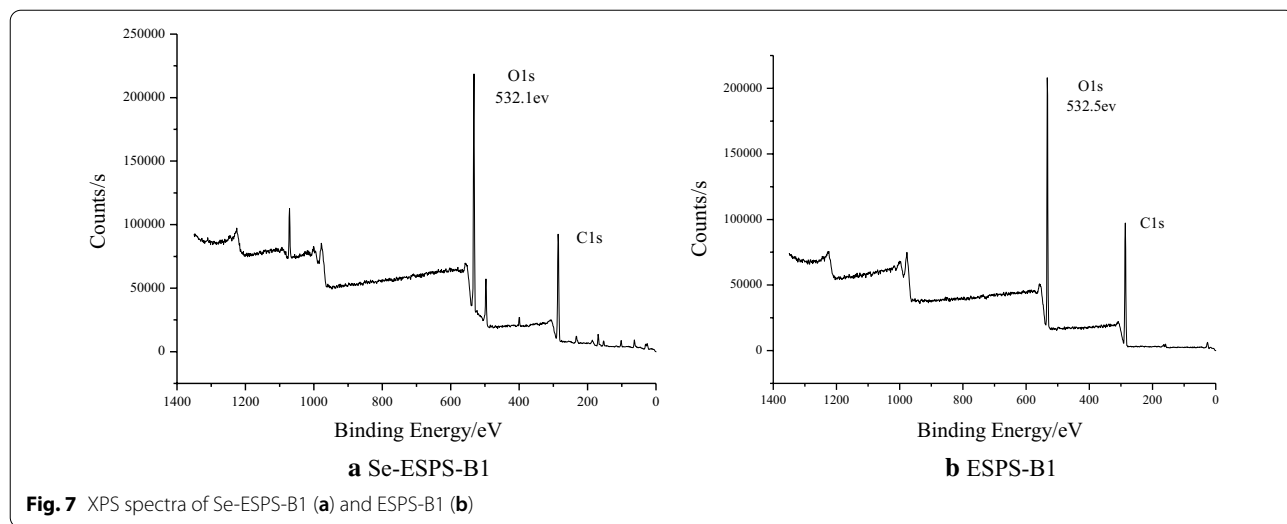
significant C1s and O1s peaks, indicating that the main components of the tested substance were C, O, and H. According to the elemental composition, the main components were inferred carbohydrates. Furthermore, the O1s binding energy of Se-ESPS-B1 (532.1 eV) was lower than that of ESPS-B1 (532.5 eV), which indicated that the introduction of selenium caused the change of electron cloud density of O atom in the polysaccharide. When Se=O replaced the hydroxyl hydrogen on the half-acetal oxygen ring, Se atom contributed electrons to increase the density of the electron cloud on the half-acetal oxygen ring. Further, the density of oxygen electron cloud on half-acetal oxygen ring increased and reduced the binding force of O atom to bind the remaining electrons in the orbital, resulting in the decrease of the binding energy [40].

Besides, the above conclusion could be verified by the Se3d spectra of Se-ESPS-B1 and ESPS-B1. Figure 8 showed that the Se3d peak of Se-ESPS-B1 was much higher than that of ESPS-B1, which indicated that more Se was introduced into the polysaccharide molecules, and the Se3d binding energy of Se-ESPS-B1was 58.18 eV, while that of ESPS-B1 was 51.53 eV. The results showed that Se atoms provided outer electrons to O atoms after entering into the internal molecular structure of polysaccharides, which reduced the binding energy of O1s and increased the binding energy of Se3d. Therefore, it could be speculated that Se formed a chemical bond with the O atom in the polysaccharide molecule. It was consistent with the result of FTIR spectra.

Moreover, the results of XPS could effectively explain the conclusion that the thermal stability of Se-ESPS-B1 was worse than that of ESPS-B1: When Se atoms were introduced into ESPS-B1 molecular chain structure in the form of $HSeO_3^-$, it had the strong electron supply ability, which reduced C–O bonding energy in Se-ESPS-B1 molecule chains and C-O bond in Se-ESPS-B1 could be easily broken, causing Se-ESPS-B1 decomposed earlier than ESPS-B1 in the thermogravimetric analysis.

SEM image results

Figure 9 showed the SEM images of Se-ESPS-B1 and ESPS-B1 at different magnifications. Under the low magnifications, Se-ESPS-B1 presented flocculent particles. From the magnification of 60,000, it could be seen that the microscopic morphology of Se-ESPS-B1 was the small and dense branch-like structure. The branches were multi-bifurcated, quasi-circular, and quasi-spherical, and the surface is smooth and non-porous. The morphology of Se-ESPS-B1 was similar to that of microcrystalline [38, 41]. Meanwhile, the microscopic morphology of ESPS-B1 was sheet-like and rod-shaped, with a smooth surface

and no bifurcation, which suggested that the interaction between ESPS-B1 molecules was strong and the binding was tight. In addition to the Se-O bond and C-O-Se bond between selenium and polysaccharides, the difference in microscopic morphology between Se-ESPS-B1 and ESPS-B1 may be due to the changes of internal hydrogen bond and intermolecular van der Waals force caused by the introduction of selenium [42, 43].

Antioxidant activity assays of Se-ESPS-B1

DPPH scavenging method is widely used for quantitative evaluation of free radical scavenging capacity of bioactive substances because of its simplicity and sensitivity. As shown in Fig. 10a, when Se-ESPS-B1 concentration was 0.2 mg/mL, the DPPH scavenging rate was 60.5%. After that, the DPPH radical scavenging rate gradually raised with the increase of Se-ESPS-B1 concentration and reached 89.7% at the Se-ESPS-B1 concentration of 1.0 mg/mL. It could also be seen that Se-ESPS-B1 could significantly scavenge DPPH radical, compared with that of ESPS-B1.

ABTS scavenging method is another effective approach to detect the free radical scavenging ability of potential antioxidants. It could be seen observed from Fig. 10b that ABTS radical scavenging rate raised with the increase of Se-ESPS-B1 and ESPS-B1 concentrations. The highest ABTS radical scavenging rate of Se-ESPS-B1 reached 85.2%. Moreover, the ABTS radical scavenging ability of Se-ESPS-B1 was significantly higher than that of ESPS-B1.

·OH scavenging method is of great significance for revealing active ingredients in treating certain diseases and delaying aging. Figure 10c indicated that ·OH radical scavenging rate was positively correlated with Se-ESPS-B1 concentrations. When the concentration of Se-ESPS-B1 was 0.2 mg/mL, the ·OH radical scavenging rate was low, but when the concentration exceeds 0.4 mg/ml, the ·OH radical scavenging rate was significantly improved. At 1.0 mg/mL, the ·OH radical scavenging rate reached 79.9%. Similarly, the ·OH radical scavenging rate of Se-ESPS-B1 was higher than that of ESPS-B1.

In general, the stronger the reduction ability implies the stronger the antioxidant activity. Figure 10d displayed that the reduction abilities of Se-ESPS-B1 and ESPS-B1 increased with the increase of concentration, showing a dose-dependent relationship. At the same dose, the reduction ability of Se-ESPS-B1is significantly higher than that of ESPS-B1. When the concentration of Se-ESPS-B1 was 1.0 mg/mL, the maximum reduction capacity was 0.54.

Similar to the above results, many studies have demonstrated that selenium-polysaccharide exhibits the

Dong *et al. Appl Biol Chem*   *(2021) 64:59*

Page 11 of 14
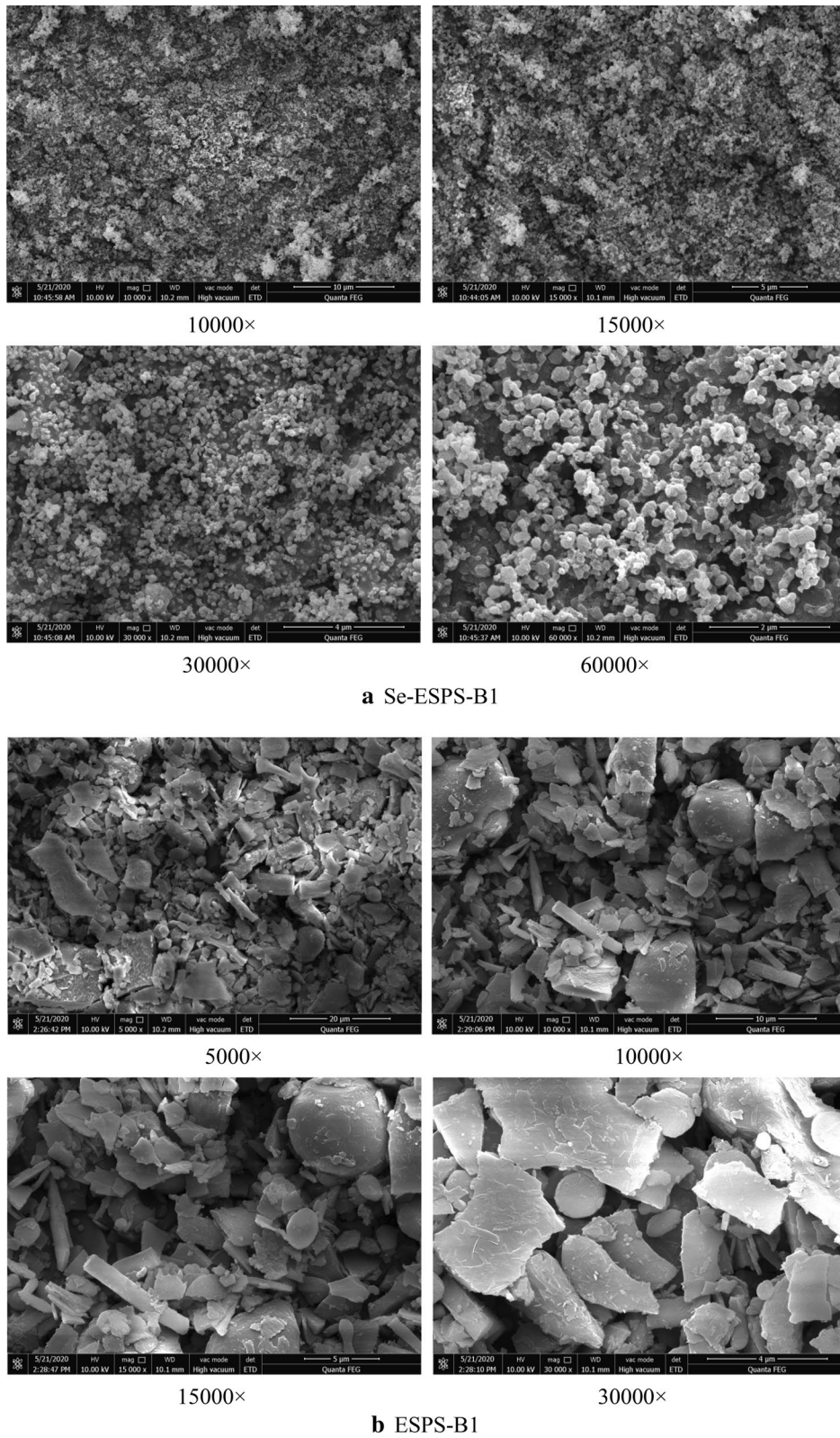
Fig. 9 SEM micrographs of Se-ESPS-B1 (**a**) and ESPS-B1 (**b**) under the different magnifications

Dong *et al. Appl Biol Chem*   (2021) 64:59

Page 12 of 14
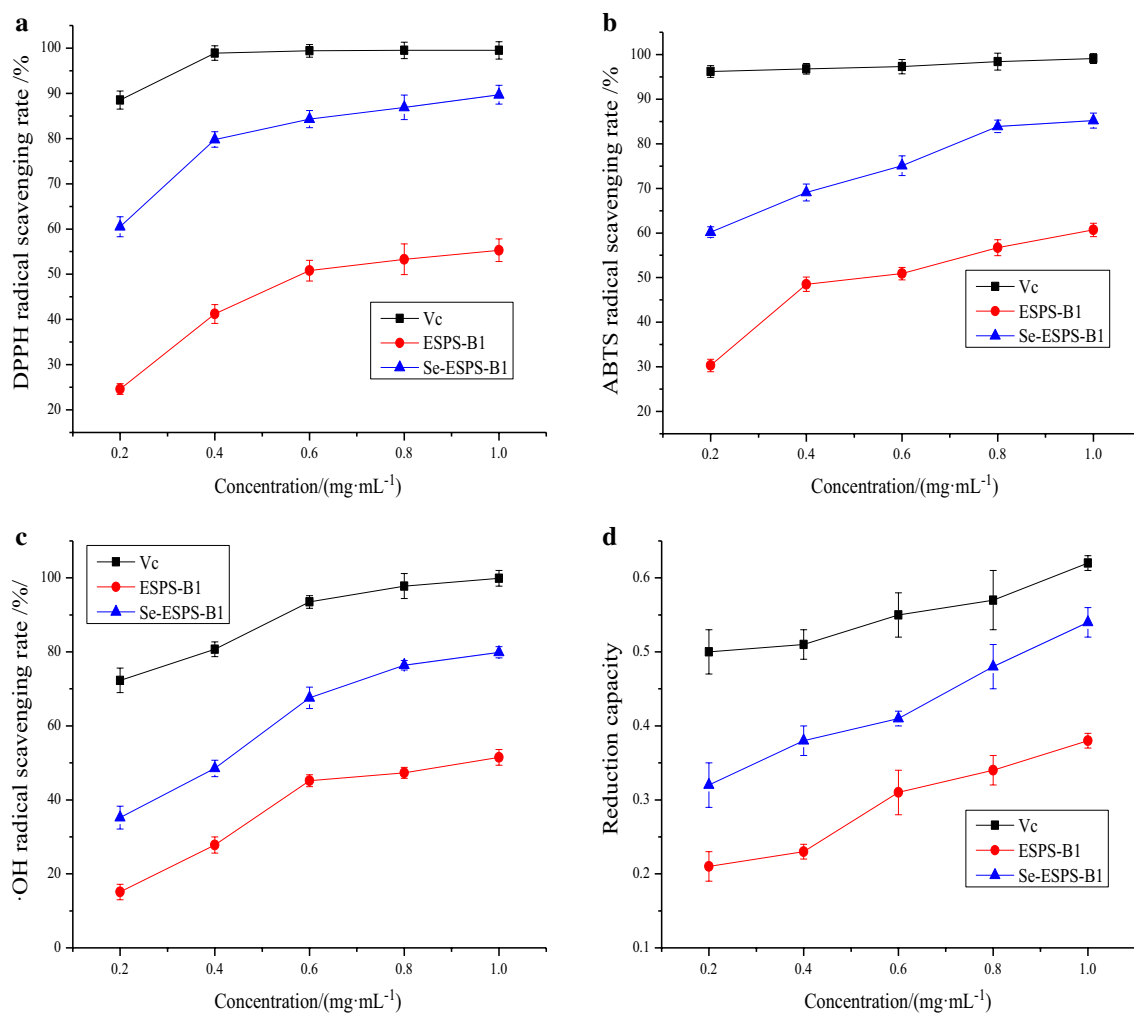
Fig.10 The levels of DPPH radical scavenging (**a**), ABTS radical scavenging (**b**), ·OH radical scavenging (**c**), and reduction ability (**d**) of Se-ESPS-B1 and ESPS-B1

antioxidant activity in vitro [44–47]. The possible chemical mechanisms for the antioxidant activity were shown as follows: firstly, the hydroxyl groups in Se-ESPS-B1 and ESPS-B1 were reacted with ferric iron, which reduced the production of free radicals induced by ferric iron [48]. Secondly, selenium in Se-ESPS-B1 could also directly trap the electrophilic free radicals [49]. Besides, compared with ESPS-B1, Se-ESPS-B1 showed significant antioxidant activity in vitro. It could also be concluded from the above results that Se-ESPS-B1 after selenization has the dual antioxidant activities of polysaccharide and selenium.

Authors' contributions
FD and ZHZ designed the experiment, analyzed the data and wrote the original draft. WSJ and SKC analyzed the results and checked the manuscript. ZYQ and XZ detected the characterzation. CL detected the antioxidant activity in vitro. QX implemented response surface design. FF supervised and guided the experiment and writing process. All authors read and approved the final manuscript.

Dong *et al. Appl Biol Chem*   (2021) 64:59

Page 13 of 14

Author details
[1]School of Health Sciences, Jiangsu Food and Pharmaceutical Science College, Huai'an 223003, China. [2]School of Pharmacy, Harbin University of Commerce, Harbin 150076, China. [3]School of Food Science and Biotechnology, Kyungpook National University, Daegu 41566, Republic of Korea. [4]School of Life Sciences, University of Sussex, Brighton BN19RH, UK. [5]School of Life Science and Technology, China Pharmaceutical University, Nanjing 211198, China.

References
1. Dorszewska J, Kowalska M, Prendecki M, Piekut T, Kozłowska J, Kozubski W (2021) Oxidative stress factors in Parkinson's disease. Neural Regen Res 16(7):1383–1391
2. Keuters MH, Keksa-Goldsteine V, Dhungana H, Huuskonen MT, Pomeshchik Y, Savchenko E, Korhonen PK, Singh Y, Wojciechowski S, Lehtonen Š, Kanninen KM, Malm T, Sirviö J, Muona A, Koistinaho M, Goldsteins G, Koistinaho J (2021) An arylthiazyne derivative is a potent inhibitor of lipid peroxidation and ferroptosis providing neuroprotection in vitro and in vivo. Sci Rep 11(1):3518
3. Mangiapane E, Pessione A, Pessione E (2014) Selenium and selenoproteins: an overview on different biological systems. Curr Protein Pept Sci 15(6):598–607
4. Liu L, Wu C, Chen D, Yu B, Huang Z, Luo Y, Zheng P, Mao X, Yu J, Luo J, Yan H, He J (2020) Selenium-enriched yeast alleviates oxidative stress-induced intestinal mucosa disruption in weaned pigs. Oxid Med Cell Longev 2020:5490743
5. Xu HB, Zhang LP, Fan HH, Sun J, Wang XW, Hu SZ (1989) A study on the interaction between selenium compounds and lipid peroxy radical. Acta Chim Sinica 47(9):901–906
6. Barbosa NV, Nogueira CW, Nogara PA, de Bem AF, Aschner M, Rocha JBT (2017) Organoselenium compounds as mimics of selenoproteins and thiol modifier agents. Metallomics 9(12):1703–1734
7. Qazi IH, Angel C, Yang H, Pan B, Zoidis E, Zeng CJ, Han H, Zhou GB (2018) Selenium, selenoproteins, and female reproduction: a review. Molecules 23(12):3053
8. Ren X, Zou L, Lu J, Holmgren A (2018) Selenocysteine in mammalian thioredoxin reductase and application of ebselen as a therapeutic. Free Radic Biol Med 127:238–247
9. Busker S, Page B, Arnér ESJ (2020) To inhibit TrxR1 is to inactivate STAT3-Inhibition of TrxR1 enzymatic function by STAT3 small molecule inhibitors. Redox Biol 36:101646
10. Jovanović M, Zhukovsky D, Podolski-Renić A, Žalubovskis R, Dar'in D, Sharoyko V, Tennikova T, Pešić M, Krasavin M (2020) Further exploration of DVD-445 as a lead thioredoxin reductase (TrxR) inhibitor for cancer therapy: optimization of potency and evaluation of anticancer potential. Eur J Med Chem 191:112119
11. Wang J, Zhao S, Yang L, Gong H, Li H, Nima C (2020) Assessing the health Loss from Kashin-Beck disease and its relationship with environmental selenium in Qamdo district of Tibet, China. Int J Environ Res Public Health 18(1):11
12. Wang S, Yan R, Wang B, Meng P, Tan W, Guo X (2019) The functional analysis of selenium-related genes and magnesium-related genes in the gene expression profile microarray in the peripheral blood mononuclear cells of Keshan disease. Biol Trace Elem Res 192(1):3–9
13. Kiełczykowska M, Kocot J, Paździor M, Musik I (2018) Selenium-a fascinating antioxidant of protective properties. Adv Clin Exp Med 27(2):245–255
14. Ahmed D, Khan MI, Sharma M, Khan MF (2018) Novel pentacyclic triterpene isolated from seeds of *Euryale Ferox* Salisb. ameliorates diabetes in streptozotocin induced diabetic rats. Interdiscip Toxicol 11(4):275–288
15. Zhang WN, Su RN, Gong LL, Yang WW, Chen J, Wang YRY, Pan WJ, Lu YM, Chen Y (2019) Structural characterization and in vitro hypoglycemic activity of a glucan from *Euryale ferox* Salisb. seeds. Carbohydr Polym 209:363–371
16. Wu CY, Wang H, He XX, Wu DW, Yue W, Wu QN (2017) The hypoglycemic and antioxidant effects of polysaccharides from the petioles and pedicels of *Euryale ferox* Salisb. on alloxan-induced hyperglycemic mice. Food Funct 8(10):3803–3813
17. Huang S, Yang W, Huang G (2020) Preparation and activities of selenium polysaccharide from plant such as *Grifola frondosa*. Carbohydr Polym 242:116409
18. Wang J, Yang X, Bao A, Liu X, Zeng J, Liu X, Yao J, Zhang J, Lei Z (2017) Microwave-assisted synthesis, structure and anti-tumor activity of selenized *Artemisia sphaerocephala* polysaccharide. Int J Biol Macromol 95:1108–1118
19. Yang W, Huang G, Huang H (2020) Preparation and structure of polysaccharide selenide. Ind Crops Prod 154:112630
20. Hamid M, Liu D, Abdulrahim Y, Khan A, Qian G, Huang K (2017) Inactivation of kupffer cells by selenizing *Astragalus* polysaccharides prevents CCl_4-induced hepatocellular necrosis in the male wistar rat. Biol Trace Elem Res 179(2):226–236
21. Gao P, Bian J, Xu S, Liu C, Sun Y, Zhang G, Li D, Liu X (2020) Structural features, selenization modification, antioxidant and anti-tumor effects of polysaccharides from alfalfa roots. Int J Biol Macromol 149:207–214
22. Zhu S, Hu J, Liu S, Guo S, Jia Y, Li M, Kong W, Liang J, Zhang J, Wang J (2020) Synthesis of Se-polysaccharide mediated by selenium oxychloride: structure features and antiproliferative activity. Carbohydr Polym 246:116545
23. Liu X, Xu S, Ding X, Yue D, Bian J, Zhang X, Zhang G, Gao P (2020) Structural characteristics of *Medicago Sativa* L. polysaccharides and Se-modified polysaccharides as well as their antioxidant and neuroprotective activities. Int J Biol Macromol 147:1099–1106
24. Cao L, Yu M, Wang C, Bao Y, Zhang M, He P, Zhang Y, Yang T, Li L, Li G, Gong Y (2019) Cellulase-assisted extraction, characterization, and bioactivity against rheumatoid arthritis of *Astragalus* polysaccharides. Int J Polym Sci 2019:8514247
25. Almajed A, Srirama D, Moghal AAB (2021) Response surface method analysis of chemically stabilized fiber-reinforced soil. Materials 14(16):1535
26. Hadidi M, Amoli PI, Jelyani AZ, Hasiri Z, Rouhafza A, Ibarz A, Khaksar FB, Tabrizi ST (2020) Polysaccharides from pineapple core as a canning by-product: extraction optimization, chemical structure, antioxidant and functional properties. Int J Biol Macromol 163:2357–2364
27. Kazemi M, Khodaiyan F, Hosseini SS (2019) Eggplant peel as a high potential source of high methylated pectin: ultrasonic extraction optimization and characterization. LWT 105:182–189
28. Lian KX, Zhu XQ, Chen J, Liu G, Gu XL (2018) Selenylation modification: enhancement of the antioxidant activity of a *Glycyrrhiza uralensis* polysaccharide. Glycoconj J 35(2):243–253
29. Bouabid K, Lamchouri F, Toufik H, Faouzi MEA (2020) Phytochemical investigation, in vitro and in vivo antioxidant properties of aqueous and organic extracts of toxic plant: *Atractylis gummifera* L. J Ethnopharmacol 253:112640
30. Zhu M, Huang Y, Wang Y, Shi T, Zhang L, ChenY XM (2019) Comparison of (poly) phenolic compounds and antioxidant properties of pomace extracts from kiwi and grape juice. Food Chem 271:425–432
31. Vasyliev GS, Vorobyova VI, Linyucheva OV (2020) Evaluation of reducing ability and antioxidant activity of fruit pomace extracts by spectrophotometric and electrochemical methods. J Anal Methods Chem 2020:8869436
32. Ji YB, Dong F, Yu M, Qin L, Liu D (2013) Optimization of synthesis of seleno-*Sargassum fusiforme* (Harv.) Setch. polysaccharide by response surface methodology, its characterization, and antioxidant activity. J Chem 2013:493524
33. Wang B, Xu Y, Chen L, Zhao G, Mi Z, Lv D, Niu J (2020) Optimizing the extraction of polysaccharides from *Bletilla ochracea* Schltr. using response

Dong *et al. Appl Biol Chem*   (2021) 64:59

Page 14 of 14

surface methodology (RSM) and evaluating their antioxidant activity. Processes 8(3):341

34. Ahmad A, Rehman MU, Wali AF, El-Serehy HA, Al-Misned FA, Maodaa SN, Aljawdah HM, Ahmad MTMP (2020) Box-Behnken response surface design of polysaccharide extraction from *Rhododendron arboretum* and the evaluation of its antioxidant potential. Molecules 25(17):3835

35. Wang Y, Wang X, Xiong Y, Fan J, Zheng Z, Li Y, Dong L, Zhao Z (2019) Extraction optimization, separation and antioxidant activity of *Luffa cylindrica* polysaccharides. Food Bioprod Process 116:98–104

36. Zhou N, Long H, Wang C, Zhu Z, Yu L, Yang W, Ren X, Liu X (2020) Characterization of selenium-containing polysaccharide from *Spirulina platensis* and its protective role against Cd-induced toxicity. Int J Biol Macromol 164:2465–2476

37. Zhang Y, Zhang Z, Liu H, Wang D, Wang J, Deng Z, Li T, He Y, Yang Y, Zhong S (2020) Physicochemical characterization and antitumor activity in vitro of a selenium polysaccharide from *Pleurotus ostreatu*s. Int J Biol Macromol 165:2934–2946

38. Wang L, Li C, Huang Q, Fu X (2019) Biofunctionalization of selenium nanoparticles with a polysaccharide from *Rosa roxburghii* fruit and their protective effect against H_2O_2-induced apoptosis in INS-1 cells. Food Funct 10(2):539–553

39. Cai W, Hu T, Bakry AM, Zheng Z, Xiao Y, Huang Q (2018) Effect of ultrasound on size, morphology, stability and antioxidant activity of selenium nanoparticles dispersed by a hyperbranched polysaccharide from *Lignosus rhinocerotis*. Ultrason Sonochem 42:823–831

40. Wei Y, Zhao Q, Wu Q, Zhang H, Kong W, Liang J, Yao J, Zhang J, Wang J (2019) Efficient synthesis of polysaccharide with high selenium content mediated by imidazole-based acidic ionic liquids. Carbohydr Polym 203:157–166

41. Gu Y, Qiu Y, Wei X, Li Z, Hu Z, Gu Y, Zhao Y, Wang Y, Yue T, Yuan Y (2020) Characterization of selenium-containing polysaccharides isolated from selenium-enriched tea and its bioactivities. Food Chem 316:126371

42. Mobika J, Rajkumar M, Sibi LSP, Priya NV (2021) Investigation on hydrogen bonds and conformational changes in protein/polysaccharide/ceramic based tri-component system. Spectrochim Acta A Mol Biomol Spectrosc 5(244):118836

43. Yang YL, Guo SJ, Zhang ZX, Zhang Y, Liu A, Xie LL, Zheng YZ (2018) Structural elucidation of galactomannan from seeds of *Crotalaria mucronata* Desv. by atomic force microscopy. Mol Med Rep 17(3):3870–3876

44. Jalali S, Montazer M, Rad MM (2021) Biologically active PET/polysaccharide-based nanofibers post-treated with selenium/tragacanth gum nanobiocomposites. Carbohydr Polym 251:117125

45. Ma L, Zhao Y, Yu J, Ji H, Liu A (2018) Characterization of Se-enriched *Pleurotus ostreatus* polysaccharides and their antioxidant effects in vitro. Int J Biol Macromol 111:421–429

46. Zhao B, Zhang J, Yao J, Song S, Yin Z, Gao Q (2013) Selenylation modification can enhance antioxidant activity of *Potentilla anserina* L. polysaccharide. Int J Biol Macromol 58:320–328

47. Liu X, Gao Y, Li D, Liu C, Jin M, Bian J, Lv M, Sun Y, Zhang L, Gao P (2018) The neuroprotective and antioxidant profiles of selenium-containing polysaccharides from the fruit of *Rosa laevigata*. Food Funct 9(3):1800–1808

48. Zhou N, Long H, Wang C, Yu L, Zhao M, Liu X (2020) Research progress on the biological activities of selenium polysaccharides. Food Funct 11(6):4834–4852

49. Kora AJ (2018) Tree gum stabilised selenium nanoparticles: characterisation and antioxidant activity. IET Nanobiotechnol 12(5):658–662

Publisher's Note